

Accounting for Hydroclimatic Properties in Flood Frequency Analysis Procedures

Joeri B. Reinders¹, Samuel E. Munoz^{2,3}

¹ Leiden University College, Leiden University, The Hague, The Netherlands.

5 ² Department of Marine and Environmental Sciences, Marine Science Center, Northeastern University, Nahant, MA 01908, USA.

³ Department of Civil and Environmental Engineering, Northeastern University, Boston, MA, USA.

Correspondence to: Joeri B. Reinders (j.b.reinders@luc.leidenuniv.nl)

10

Abstract. Flood hazard is typically evaluated by computing extreme flood probabilities from a flood frequency distribution following nationally defined procedures in which observed peak flow series are fit to a parametric probability distribution. These procedures, also known as flood frequency analysis, typically recommend only one probability distribution family for all watersheds within a country or region. However, large uncertainties associated with extreme flood probability estimates (> 50 -year-flood or Q_{50}) can be further biased when fit to an inappropriate distribution model because of differences in the tails between distribution families. Here, we demonstrate that hydroclimatic parameters can aid the selection of a parametric flood frequency distribution. We use L-moment diagrams to visually show the fit of gaged annual maxima series across the United States, grouped by their Köppen climate classification and the precipitation intensities of the basin, to a General Extreme Value (GEV), Log Normal 3 (LN3) and Pearson 3 (P3) distribution. Our results show that basic hydroclimatic properties of a basin exert a significant influence on the statistical distribution of the annual maxima. The best-fitted family distribution shifts from an GEV towards an LN3 distribution across a gradient from colder and wetter climates (Köppen group D, continental climates) towards more arid climates (Köppen group B, dry climates). Due to the diversity of hydrologic processes and flood generating mechanisms among watersheds within large countries like the United States, we recommend that the selection of distribution model be guided by the hydroclimatic properties of the basin rather than relying on a single national distribution model.

15

20

25

1. Introduction

30 Around the world, communities depend on rivers for vital resources, yet riverine floods present a significant hazard for people and infrastructure along interior waterways (Mallakpour and Villarini, 2015; Peterson et al., 2013). To mitigate risks and develop safe emergency plans, water managers depend on reliable methods to compute extreme flood probabilities. Typically these methods use the probability distribution of annual maxima discharge, also
35 known as the flood frequency distribution, from which one can compute extreme flood probabilities (e.g., the 100-year flood (Q100), a flood with a 1% chance of occurrence in a given year) (Hamed and Ramachandro Rao, 2000; Kidson and Richards, 2005; Cassalho et al., 2019). To construct flood frequency distributions, national flood frequency procedures around the world fit observed annual stream maxima to a parametric probability distribution model (Castellarin et al., 2012; Madsen et al., 2014). These approaches involve and are affected by, the a priori
40 assumption of what parametric statistical model best captures the empirical distribution of flood magnitudes (Kidson and Richards, 2005). Standard national procedures often prescribe just one probabilistic distribution model, for example, the United States Bulletin 17C recommends the Log-Pearson III (LP3) distribution family (England et al., 2019), while in the United Kingdom, the FEH (Flood Estimation Handbook) recommends the use of the General Logistic distribution (GLO) (Robson and Reed, 1999). Although these recommendations provide a
45 consistent framework for flood frequency analyses (Barth et al., 2019), they can also result in biased estimates of infrequent flood probabilities when applied over large hydro-climatically diverse regions (Klemes, 1993; Merz and Bloschl, 2003, 2008), due to the inherent differences in the distribution shape and tail thickness of different parametric models. These differences can amplify the already large uncertainties for extreme flood probability estimates, such as the hundred- or five-hundred-year floods.

50 Watershed morphology, land use management, and climatology affect flood frequency properties such as the mean, variance, and tails or respectively the location, scale, and shape parameters of the probabilistic distribution. For example, large watersheds have the capacity to absorb heavy precipitation events better than small watersheds (Iacobellis et al., 2002; Salinas et al., 2014b), meaning that peak flow in smaller watersheds is disproportionately
55 affected by an extreme precipitation event and that they observe higher peak flow variances (Iacobellis et al., 2002; Salinas et al., 2014a). Other studies have noted more complex relationships, where the variance of flood frequency distributions decreases with watershed area for small watersheds, but increases with area for large watersheds (Bloschl and Sivapalan, 1997; Smith, 1992). Urbanization leads to a reduction in soil permeability and an increase in precipitation-induced surface runoff (Hall et al., 2014; Hodgkins et al., 2019), which results in more local flash
60 floods that are associated with thick-tailed flood frequency distributions (Merz and Bloschl, 2003; Zhang et al., 2018). Relatedly, population growth (a proxy for urbanization) and river engineering (e.g., channel straightening) can increase mean annual peak flows (Villarini et al., 2009; Munoz et al., 2018).

65 Local flood-generating mechanisms, particularly the type, duration, and intensity of local precipitation events, affect all aspects of the flood frequency distribution (Hall et al., 2014; Merz and Bloschl, 2003). In watersheds where precipitation occurs predominantly as rain as opposed to snow, flood frequency distributions exhibit higher variance (Merz and Bloschl, 2003; Gaal et al., 2015). Similarly, watersheds where total annual precipitation only falls in a few intense events also have flood distributions with high variances (Bloschl and Sivapalan, 1997; Pitlick, 1994), whereas watersheds with high total annual precipitation observe flood distributions with lower variances
70 (Salinas et al., 2014b). Merz and Bloschl (2003) summarized several of these findings in their typology of regional flood-generating mechanisms. Antecedent soil moisture adds another level of complexity to the relationship between precipitation and flood frequency distribution shape, as synchronicity between precipitation and antecedent soil moisture levels is likely to thicken the flood frequency distribution tails through surface runoff levels (Ivancic and Shaw, 2015).

75 The patterns between local watershed characteristics and flood frequency distribution properties form a potential tool to improve extreme flood probability estimates in hydrologically diverse regions. One method is to select a parametric distribution based on the value of an environmental parameter at the gaged location, for example a precipitation statistics or drainage area. Salinas et al. (2014b) demonstrate that European rivers with different
80 drainage areas and total annual precipitation fit differently to multiple three-and-two-parameter distribution families. However, as described above, the relation between drainage area and flood frequency shape is complex, and annual maximum rainfall does not necessarily reflect different precipitation regimes. There are relatively few studies that relate flood frequency distributions to aggregated climate classifications such as the Köppen climate regions (Kottek et al., 2006; Peel et al., 2007). In one such study, Metzger et al. (2020) demonstrate that flood
85 frequency distributions in arid and semi-arid regions give larger 10 to 100-year flood ratios compared to Mediterranean climates; a similar relation was found when arid regions are compared to humid regions (Zaman et al., 2012). These findings provide strong support for the hypothesis that the hydroclimatic properties of a basin

- particularly aggregate hydroclimatic classifications like the Köppen system - influence the tail thickness of flood frequency distributions and thus exert considerable influence on the probabilities of the most extreme flood events.

Here we build on the previous work by Salinas et al. (2014a, 2014b) by examining the fit of annual maxima streamflow data from across the United States to several three-parameter distributions via L-moment diagrams. We perform a similar experiment, but group annual maxima gage records based on two aggregated hydroclimatic variables instead of one-dimensional variables: (1) the Köppen climate region, which are based on temperature and precipitation normals (Kottek et al., 2006); and (2) by watershed precipitation intensity, which is a combination of the maximum daily precipitation and the total annual precipitation. By grouping gage discharge records based on the hydroclimatic properties of their basin, we assess whether these variables can guide a priori parametric distribution model selection. Our results demonstrate that peak flow records from different Köppen climate regions and precipitation intensity groups tend to fit to specific distribution families. These findings imply that the hydroclimate properties of a watershed could be used to guide the selection of a distribution family in flood frequency analysis.

2. Hydroclimatic Data & Methodology for the L-moment Diagrams

2.1. Data

We chose the United States for our study because it spans all of the five main Köppen climate groups (Peel et al., 2007) and has watersheds that are influenced by a diverse set of synoptic weather systems (Hirschboeck, 1988). Yet, despite this hydroclimatic diversity, the LP3 distribution is recommended for all flood frequency analyses in the United States in Bulletin 17C (England et al., 2019). To determine the flood frequency distribution shape of different United States rivers, we constructed a dataset containing 1538 annual maxima discharge records (Fig. 1 a). This dataset is a selection of the larger USGS surface water database which contains observational data from a network of gages across the United States (USGS, 2020). To generate our dataset, we first selected all records longer than 30 years. Next, we picked the longest continuous record for each independent USGS hydrologic unit, to avoid biasing the distribution selection towards more heavily sampled rivers. We also included records from Alaska and Hawaii to encompass additional hydroclimatic diversity. The annual maxima records in the final dataset have an average length of 78 years, and a range from 30 to 118 years (Fig. 1 b).

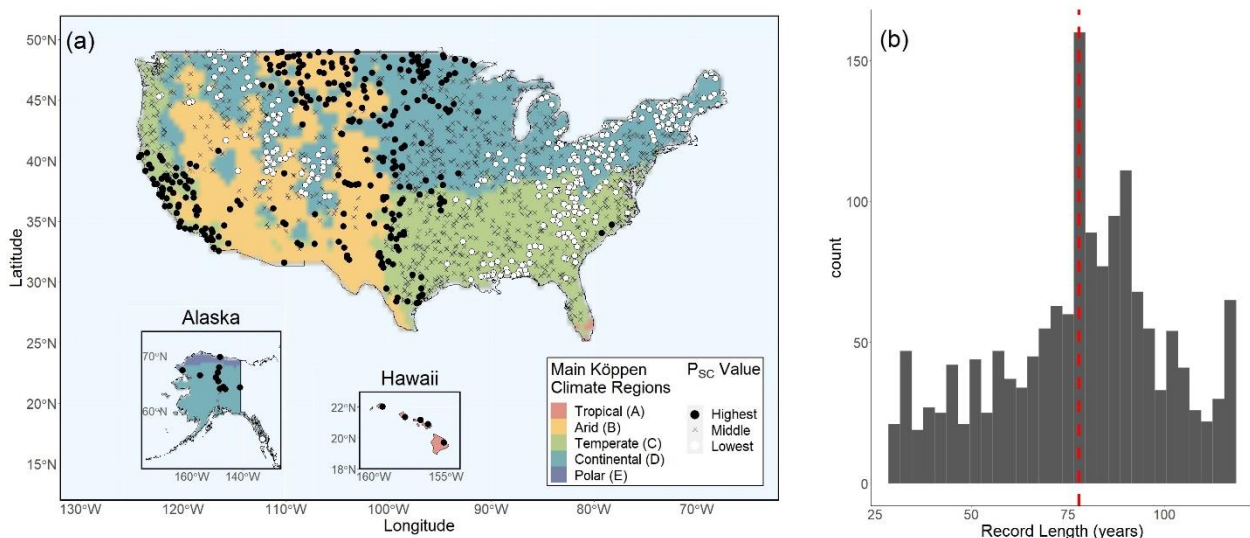


Figure 1: (a) Locations of hydrologic annual maxima records from instrumental river gages used in this study grouped by the percentage of the maximum annual daily precipitation level by the total annual precipitation level (P_{sc}) and plotted atop their Köppen climate region. (b) Histogram of discharge record length in years, the red line indicates the mean value 78 years.

To classify the gage records in different hydroclimatic groups, each annual maxima record was assigned a Köppen climate classification (Peel et al., 2007; ORNL DAAC, 2017), and a long-term (1981-2010) daily mean

precipitation record from the Climate Prediction Center (CPC) precipitation dataset based on proximity (CPC, 2020). First, annual maxima records were categorized by their main Köppen climate group: arid (B), temperate (C), or continental (D) - other climate groups did not have enough representation among the gages compared to the other climate groups (six for tropical and one for polar - all located in Hawaii or Alaska) (ORNL DAAC, 2017). Of the 1538 annual maxima, 215 are in an arid climate (Köppen group B), 578 are located in temperate climates (Köppen group C), and 738 are located in continental climates (Köppen group D). Next, we categorized annual maximum records by their watershed's hydroclimatic intensity, defined here as the percentage contribution of the maximum daily precipitation level to the total annual precipitation (P_{SC}) in the CPC record (CPC, 2020). Gages close to high P_{SC} values thus experience most precipitation during high intensity events, whereas gages with low P_{SC} values experience precipitation more evenly throughout the year. We also assessed other precipitation metrics (e.g. annual maximum daily precipitation and the 95th percentile of the daily precipitation level distribution) but these metrics were not as meaningfully associated with flood distributions as P_{SC} , which is similar to precipitation metrics known to influence flood frequency distribution shape (Metzger et al., 2020; Pitlick, 1994). Each annual maxima record was assigned to one of three groups: the lowest 20% P_{SC} values containing 308 records (i.e., precipitation spread more evenly throughout the year), the highest 20% P_{SC} values containing 308 records (i.e., a significant proportion of annual precipitation falls in one storm), and all intermediate values encompassing the remaining 922 records. The 20th and 80th percentiles were chosen, because they preserve a meaningful difference between the two groups while maintaining large sample sizes.

2.2. L-Moment Diagrams

We use L-moment diagrams to measure the fit of annual maxima records to several parametric distribution families. L-moment diagrams are a graphical tool to assess the goodness-of-fit of multiple annual maxima records to a series of probabilistic models and guide the selection of a regional flood frequency distribution family (Peel et al., 2001; Vogel and Fennessey, 1993). The L-moments of a hydrologic record are the linear combinations of its order statistics and, like regular moments (i.e. the mean, standard deviation, and skewness) describe the shape of a sample distribution. A detailed description of L-moments and how to compute them is given by Hosking and Wallis (1997). L-moments are often preferred over regular moments because they are more robust to small sample sizes (Hosking, 1990; Wang, 1990). A L-moment diagram is constructed by plotting the L-moment coefficient of skewness (L-Cs) against the corresponding L-moment coefficient for kurtosis (L-Ck) (Hosking and Wallis, 1997). Consequently, any 3-parameter distribution can be plotted as a line in the L-moment diagram from their mathematical formulation of the ratio between L-Cs and L-Ck (Table 1). The distance between the L-Cs and L-Ck of a sample and the line describing a particular 3-parameter distribution represents the likelihood of the record deriving from that distribution - the closer the sample to the line, the better the fit (Hosking and Wallis, 1997).

Table 1: Overview of the distributions used in this study including their probability density function and L-moments (ratios)

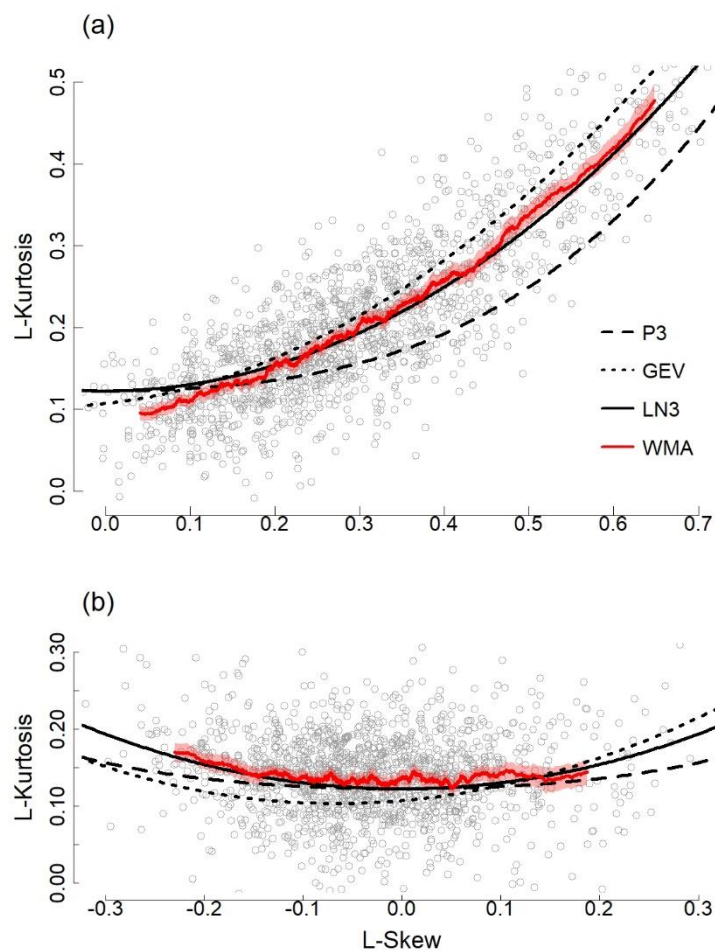
| Name | Probability Density Function | L-moments and L-moment ratios |
|--|--|--|
| Generalized Extreme Value Distribution (GEV) | $f(x) = \frac{1}{\alpha} e^{-(1-k)y - e^{-y}}, y = \begin{cases} -\frac{1}{k} \log \left\{ 1 - k \left(\frac{x-\xi}{\alpha} \right) \right\}, k \neq 0 \\ \frac{x-\xi}{\alpha}, k = 0 \end{cases}$ | $\lambda_1 = \xi + \alpha \frac{\{1 - \Gamma(1+k)\}}{k}, \lambda_2 = \frac{\alpha(1 - \frac{k}{2})\Gamma(1+k)}{k}$ $\tau_3 = 2 \frac{(1-3^{-k})}{(1-2^{-k})} - 3$ $\tau_4 = \frac{5(1-4^{-k}) - 10(1-3^{-k}) + 6(1-2^{-k})}{(1-2^{-k})}$ |
| Log-Normal 3-parameter Distribution (LN3) | $f(x) = \frac{e^{ky - y^2/2}}{\alpha\sqrt{2\pi}}, y = \begin{cases} -\frac{1}{k} \log \left\{ 1 - k \left(\frac{x-\xi}{\alpha} \right) \right\}, k \neq 0 \\ \frac{x-\xi}{\alpha}, k = 0 \end{cases}$ | $\lambda_1 = \xi + \alpha \frac{\{1 - e^{\frac{k^2}{2}}\}}{k}, \lambda_2 = \frac{\alpha}{k} e^{\frac{k^2}{2}} \left\{ 1 - 2\Phi\left(\frac{-k}{\sqrt{2}}\right) \right\}$ |
| Pearson Type III Distribution | $f(x) = \frac{(x-\xi)^{\alpha-1} e^{-(x-\xi)/\beta}}{\beta^\alpha \Gamma(\alpha)}$ $\alpha = \frac{4}{\gamma^2}$ $\beta = \frac{1}{2} \sigma \gamma , \gamma \neq 0$ $\xi = \frac{\mu - 2\sigma}{\gamma}$ | $\lambda_1 = \xi + \alpha\beta, \lambda_2 = \pi \frac{1}{2} \beta \frac{\Gamma(\alpha + \frac{1}{2})}{\Gamma(\alpha)}$ $\tau_3 = 6J_1(\alpha, 2\alpha) - 3$ |

Notes: Formulation of the probability density functions, and L-moments are taken from Hosking and Wallis (1997). For all functions 'a, and k are the location, scale and shape parameters, respectively. When t3, t4 are determined via 465 a rational function approximated, which is described in detail in Hosking and Wallis (1997).

The L-moments and L-moment ratios for each annual maxima record in our dataset are compared to a GEV, LN3 and a Pearson 3 (P3) distribution. These three parameter distributions are commonly used in hydrologic sciences

185 (Salinas et al., 2014b), and are known to fit extreme flood values in the United States well (Vogel et al., 1993; Vogel and Wilson, 1996). Additionally, we plotted Log-transformed discharge records in L-moment diagram, to fit them to a LP3 distribution. L-moment diagrams are constructed for all records in the dataset, and each selection of record based on their Köppen climate classification and P_{SC} value.

190 Prior work demonstrated that selecting one distribution that provides the best fit to annual maxima is difficult over a large hydrologically heterogeneous region due to the high sample variance of the L-moments (Asikoglu, 2018; Salinas et al., 2014a). To reduce the noise and guide model selection, we compute a weighted moving average (WMA) of neighboring L-Cs and their corresponding L-Ck proportional to record length. Salinas et al. (2014a) applied this method to annual maxima series from across Europe to argue for the GEV distribution as a pan-European flood frequency distribution. We computed the WMA and its 95% confidence interval to summarize sample variance and facilitate distribution selection of all L-moment diagrams in this study. The weighted averages are taken from 50 consecutive L-Cs's and of the 50 corresponding L-Ck's proportional to record length.



200 **Figure 2: L-moment diagrams with the L-moment ratio for skew and kurtosis of annual maxima records used in this study (gray dots; n=1538), with their weighted moving average (WMA) proportional to record length (red line) and the P3, GEV and LN distribution lines: (a) annual discharge maxima as recorded by the gage, and; (b) the logarithm of the annual discharge maxima.**

3. Results

205 The WMAs demonstrate that the average statistical properties of the 1538 L-moment ratios across the United States are best characterized by the LN3 distribution, with large variance among individual records (Fig. 2). Specifically, the WMA of the largest L-Cs and L-Ck follow the LN3 distribution line as opposed to the P3 and GEV distributions (Fig. 2a). Generally, these originate from rivers for which the discharge of the extreme flood is relatively large compared to the average annual flood peak – in other words a distribution with a thick tail. The WMA deviates from the LN3 distribution as L-moment ratios become smaller, after which L-moments are better characterized by

the GEV distribution (Fig. 2a). The theoretical distribution lines are more clustered for these smaller L-moment ratios, reflecting the similarities of GEV and LN3 distributions for thin-tailed distributions with low skewness (Fig. 2a). In log-space, clustering of L-moment ratios around the LP3 distribution supports the general use of this distribution for rivers in the United States (England et al., 2019), although we note that the data more closely track the LN3 distribution, particularly for extreme values of skew and kurtosis (Fig. 2b).

When annual maxima are grouped by Köppen climate region, the WMA shifts from the best-fitted distribution line as we move from arid to more temperate climates (Fig. 3). The statistical properties of records from temperate climates are best described by the LN3 distribution (Fig. 3c), whereas records from continental regions are represented by a GEV distribution (Fig. 3e). The WMA of annual records from arid climates does not track one distribution family line: the LN3 distribution best represents records with high L-Cs values [0.5-0.7] and the P3 distribution better follows the lower L-Cs values [0.1-0.4] (Fig. 3a). We note that the smaller sample size of the arid climate group results in larger confidence intervals. The concentrations of individual L-moment ratios also shift when grouped by climate region: the clustering of L-moment ratios for continental climates is highest along the GEV distribution line (Fig. 3e), for temperate L-moment ratios it falls in between the GEV and LN3 line (Fig. 3c), and for arid L-moments between the LN3 and P3 line (Fig. 3a). A clear shift between distribution families for different climate regions is not observed in log-space, where we also find no clear best-fitted distribution along the full range of L-Cs values for any of the climate zones. Log-transformed records in arid climates exhibit overall lower L-Ck values compared to records from continental and temperate climates and are best represented by the LP3 distribution for positive L-Cs (Fig. 3b), whereas negative L-Cs values do not clearly follow one distribution. Flood distributions in temperate regions are well represented by the LN3 distribution for negative L-Cs values, and the LP3 distribution for positive L-Cs values. (Figs. 3d).

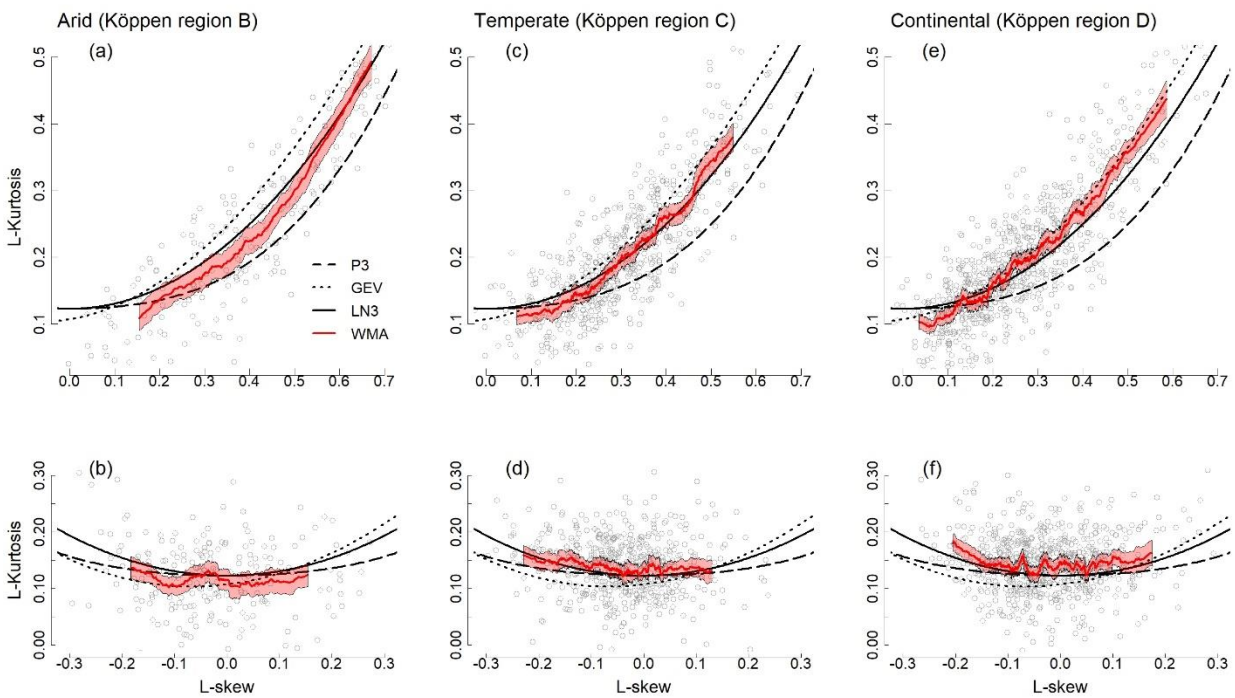


Figure 3: L-moment diagram with the L-skew and L-kurtosis for annual discharge maxima records (gray dots) grouped by their Köppen climate region, their weighted moving averages (WMA) proportional by record length (red line) and the P3, GEV and LN distribution line (striped; dotted; solid). Panels (a), (c), and (e) show annual discharge maxima as recorded by the gage; Panels (b), (d), and (f) show the logarithm of the annual discharge maxima.

Categorizing annual maxima discharge records based on different local precipitation intensities (P_{5C}) also influences the variance of L-moment coefficient (Fig. 4). The WMA of records with low precipitation intensities follows the GEV distribution line, especially for higher L-Cs values [0.2-0.45] (Fig. 4a). However, no one best-fit distribution can be assigned to high and intermediate precipitation intensity groups. The L-moment coefficients associated with high P_{5C} values follow the LN3 distribution line for L-Cs values between 0.4-0.7, whereas the WMA falls between the LN3 and P3 distribution for lower L-Cs values [0.15-0.4] (Fig. 4e). The WMAs of the intermediate group falls in between the GEV and LN3 distribution lines where for low [0-0.15] and high [0.4-0.6] L-Cs values it follows the GEV distribution, but for intermediate L-Cs values [0.15-0.4] it more closely follows

the LN3 distribution (Fig. 4c). The position of this line within the parameter space does indicating the observed shift from the GEV to the LN3 distribution as P_{SC} values increase (Fig. 4c). Additionally, the range of L-Cs values is much smaller for records with low P_{SC} values (Fig. 4a). We could not clearly distinguish a best-fitted distribution between the groups when records were log-transformed (Figs. 4b, 4d, and 4f). For the intermediate P_{SC} values the WMA line tracks the LN3 distribution line, but for the highest P_{SC} values the WMA follows both the LN3 distribution (for negative L-Cs values) and the P3 distribution (for positive L-Cs values).

Our analyses document shifts of flood distribution properties for both the Köppen climate groups and the P_{SC} groups, where arid climates (high P_{SC}) and continental climates (low P_{SC}) move away from the LN3 distribution towards the P3 and GEV distribution. In contrast, the WMAs of both the temperate and intermediate P_{SC} group trend closer to the LN3 distribution line. A major difference between these two categories is the range of L-Cs values between the corresponding groups. For example, the range of the lower P_{SC} is smaller than that of the L-moment ratios in the corresponding groups. There is no clear best-fit distribution within the arid Köppen category and the higher P_{SC} groups, as the WMA varies over the observed L-Cs range. However, we do demonstrate that regional hydroclimatic differences explain part of the variance among individual flood distributions.

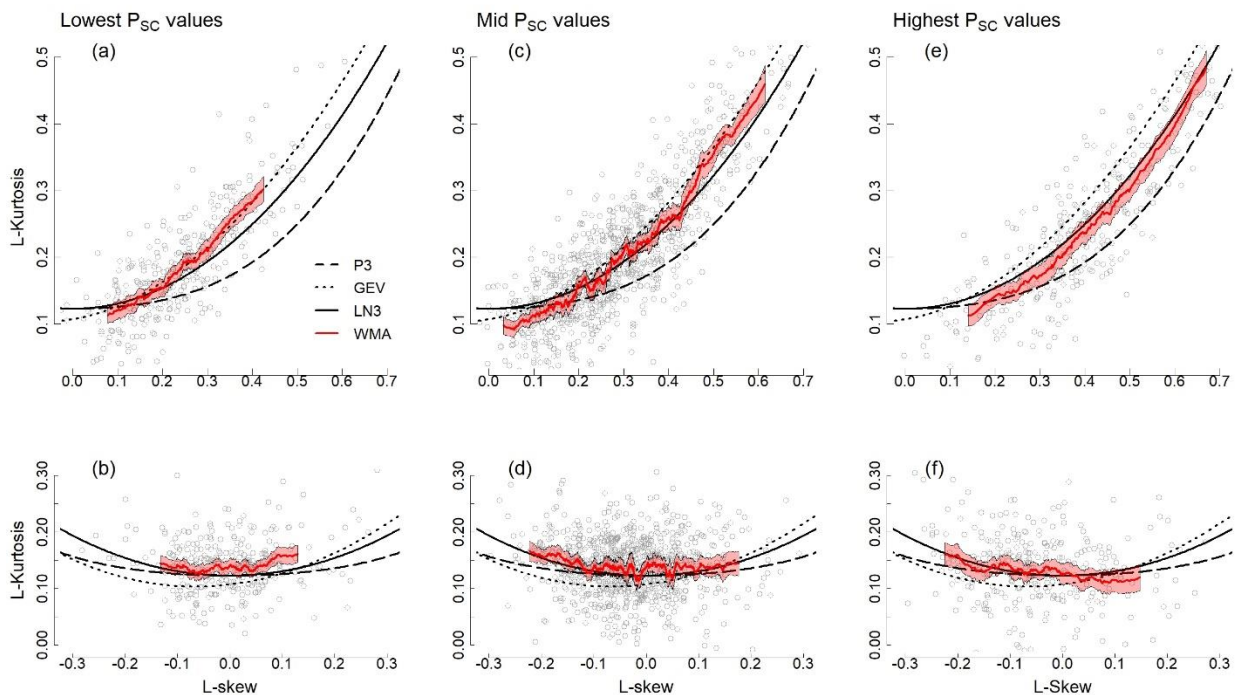


Figure 4: L-moment diagram with the L-skew and L-kurtosis for gage discharge records (gray dots) grouped by their percentage of the maximum annual daily precipitation level by the total annual precipitation level (P_{SC}), their weighted moving averages (WMA) proportional by record length (red line) and the P3, GEV and LN distribution line. Panels (a), (c), and (e) show annual discharge maxima as recorded by the gage; panels (b), (d), and (f) show the logarithm of the discharges.

4. Discussion

The main objective of this study is to evaluate whether hydroclimatic data can improve extreme flood probability estimates in flood frequency analysis procedures, through informed distribution family selection. To do this, we grouped annual hydrologic maxima from gage records across the United States by their hydroclimatic properties, and used L-moments to guide the selection of a probability model. Our work provides insights into the hydroclimatic parameters that drive flood frequency distribution shape, and how to supplement conventional flood frequency analyses using hydrological information accordingly.

4.1. Flood Frequency Distributions in the United States

The average statistical properties of annual hydrologic maxima across the United States are most closely represented by the LN3 distribution, although for records with low L-Cs values [0.05 – 0.2] the GEV distribution fits better (Fig. 2a). These findings are consistent with, and further specify, prior work by Vogel and Wilson

285 (1996), who also used L-moment diagrams to conclude that the LN3, LP3, and GEV distributions are all reasonable
representations of annual maxima across the United States. In log-space the LN3 distribution also provides the
best-fit, however the distribution lines are more similar making the log-P3 distribution an appropriate choice, as
recommended by Bulletin 17C, for records with positive L-Cs values. Bulletin 17C accounts for negatively skewed
flood distributions by censoring potentially influential low floods (PILFs) that could lead to underestimation of
extreme flood values (England et al., 2019).

290 Our analyses demonstrates that hydroclimatic factors, such as Köppen climate region and precipitation intensity,
explain part of the L-moment ratios sample variance and flood frequency distribution shapes across the United
States. The distribution family that best characterized hydrologic maxima shifts from the GEV towards the LN3
distribution as we move from cold and wet climates (Köppen group D) to warmer and drier climates (Köppen
295 group B) (Fig. 3). The contribution of the annual maximum storm to annual total precipitation (P_{SC}) shows a similar
pattern: watersheds with a lower maximum storm contribution are best captured by the GEV distribution and with
a higher P_{SC} by the LN3 distribution (Fig. 4). Although we do not provide evidence for a causal link, the flood
regimes generally associated with arid and continental hydroclimatic regions match the statistical properties of the
GEV and LN3 distribution families as described by the L-moment lines (Fig. 3 and Fig. 4). For example, arid
300 climates generally experience flash floods (high P_{SC} values) and as a result skewed flood frequency distributions
(thick tails) compared to continental climates; similarly the LN3 distribution line fits to higher L-Cs ratios for the
same L-Ck compared to the GEV distribution (Metzger et al., 2020; Zaman et al., 2012). It also fits the results of
a simulation experiment by Salinas et al. (2014a), that shows how the high variance of the L-moment ratio samples
cannot alone be attributed to sampling error, and that other covariates were needed to explain the variance. They
305 observed a shift of the best-fit distribution from GEV to LN3 as the total annual precipitation decreases over a
catchment observed by Salinas et al. (2014b) in Europe. Köppen climate regions could provide a potential
explanation for why Salinas et al. (2014b) found the GEV distribution to be the best fit for European annual
maxima, as it is a continent dominated by temperate and cold climates (Köppen groups C and D). In contrast, the
United States includes large regions with arid climates as well as temperate and cold regions, which shifts the
310 overall best fit distribution for annual maxima to the LN3 distribution.

4.2. Improvements to Flood Frequency Analysis

315 Even though watershed-specific hydroclimatic variables, such as main Köppen group, affect the variance of L-
moment ratios of annual maxima records, they did not always yield a distinct best-fit distribution family for the
constructed hydroclimatic regions in this study. The Köppen classification indirectly already includes several flood
generating variables — precipitation seasonality and intensity, vegetation, soil type, infiltration capacity, and
surface runoff levels — as they are constructed from temperature and precipitation levels (Kottek et al., 2006; Peel
et al., 2007). Accordingly, the observed results for gages grouped by Köppen climate regions are likely confounded
320 by any of these factors, including P_{SC} . As these climate classification schemes indirectly contain multiple
environmental variables and encompass large contiguous areas they form a promising tool for systematic
distribution selection in flood frequency analysis. Solely local precipitation intensities (like P_{SC}) may represent
large river systems poorly if discharge at given downstream location could be influenced by multiple precipitation
regimes from multiple tributaries. Encountering this problem becomes less likely with Köppen regions which often
325 cover entire watersheds. Yet, the high precipitation intensity (P_{SC} levels) group and the arid Köppen region generate
multiple best-fitted distribution families across the range of possible L-Cs values, implying a more detailed
classification is necessary. The annual maxima records in arid climates (Fig. 3a) and with intense precipitation
regimes (high P_{SC} values) (Fig. 4e) either best-fitted to the P3 distribution for low L-Cs values, or the LN3 for high
values. In this particular case, Köppen's specification for arid climates — BWh, BWk, BSk, and BSk — might be
330 provide a systematic method to distinguish between different types of arid regions. Additionally, one could include
other basin characteristics, specifically geomorphic properties of the watershed (e.g., size and elevation) in further
improving probability model selection, given that prior work points to hydroclimatic variables as exerting a
primary control on flood distributions (Salinas et al., 2014b). For example, Pitlick (1994) showed that the shape
parameter of flood frequency distributions in mountainous areas of the Western United States were affected by
335 regional precipitation intensity — combining climatic and geomorphic parameters.

Our main finding - that hydroclimatic properties of a basin exert a strong influence on the distribution of annual
discharge maxima - provides a potential means to improve the accuracy of extreme flood probability estimates
without altering the mathematical procedure described in flood frequency analysis guidelines like Bulletin 17C
340 (England et al., 2019). One approach to further improve on our work is the weighted mixed populations framework,
where one stratifies data and fits a parametric distribution to each new data population to aggregate the population
distributions into a single distribution weighted on population size (Barth et al., 2019). In a hydrologic context,

one could subdivide annual flood discharges based on different (periodic) flood-generating mechanisms. Accordingly, this method works particularly well for watersheds with multiple distinct flood-generating mechanisms, for example due to periodic atmospheric rivers, and skewed flood distributions (Barth et al., 2019). Another approach is to use other parametric distributions, with four or more parameters - although such methods do not explicitly consider hydrologic information- or a Metastatistical Extreme Value Distribution (MEVD) (Marani and Ignaccolo, 2015; Miniussi et al., 2020). A MEV distribution derives an extreme (annual maxima) flood frequency distribution via 'ordinary' discharge values and has shown to be efficient with all sorts of parametric distributions (Marani and Ignaccolo, 2015).

5. Conclusions

We evaluated annual hydrologic maxima distributions from across the United States, and showed that probability model selection can be improved when it is based on the hydroclimatic properties of the basin. In the United States, the WMA line of L-moment coefficients track the LN3 distribution, implying that this distribution could serve as national distribution family. However, distribution selection can be improved by taking a basin's climate region into account, where continental climates (cool/wet) are best described by GEV distributions while arid climates (hot/dry) are best described by LN3 distributions. More broadly, our work demonstrates that the climatology of a region is a powerful tool to guide the a priori distribution selection in flood frequency analysis.

Acknowledgments

We would like to thank Willem Toonen, Paul Hudson, Ed Beighley, Auroop Ganguly, Dick Bailey for valuable discussion and comments on this work. In addition, we thank dr. Félix Francés and an anonymous reviewer, who provided thorough feedback which significantly improved the manuscript. This project was supported by grants from the US National Science Foundation (EAR-1804107 and EAR-1833200).

Code availability

The R-scripts used to perform the analyses and make the figures in this paper are available from the Zenodo open respiratory <https://doi.org/10.5281/zenodo.4476066>.

Data availability

Data in this study are available through the United States Geological Survey (USGS) Water Data for the Nation (<https://waterdata.usgs.gov/nwis>). The specific dataset containing the 1538 USGS peak flow records is available via the Zenodo open respiratory <https://doi.org/10.5281/zenodo.4476066>.

References

- 385 Asikoglu, O. L.: Parent flood frequency distribution of Turkish rivers, *Polish J. Environ. Stud.*, <https://doi.org/10.15244/pjoes/75963>, 2018.
- 390 Barth, N. A., Villarini, G. and White, K.: Accounting for Mixed Populations in Flood Frequency Analysis: Bulletin 17C Perspective, *J. Hydrol. Eng.*, [https://doi.org/10.1061/\(asce\)he.1943-5584.0001762](https://doi.org/10.1061/(asce)he.1943-5584.0001762), 2019.
- Blöschl, G. and Sivapalan, M.: Process controls on regional flood frequency: Coefficient of variation and basin scale, in *Water Resources Research*, <https://doi.org/10.1029/97WR00568>, , 1997.
- 395 Cassalho, F., Beskow, S., de Mello, C. R. and de Moura, M. M.: Regional flood frequency analysis using L-moments for geographically defined regions: An assessment in Brazil, *J. Flood Risk Manag.*, <https://doi.org/10.1111/jfr3.12453>, 2019.
- 400 Castellarin, A., Kohnova, S., Gaal, L., Fleig, A., Salinas, J. L., Toumazis, A., Kjeldsen, T. R. and Macdonald, N.: Review of applied-statistical methods for flood-frequency analysis in Europe. <http://www.cost.eu/module/download/33272>, 2012.
- Climate Prediction Center (CPC): CPC Global Unified Gauge-Based Analysis of Daily Precipitation, <https://psl.noaa.gov/data/gridded/data.cpc.globalprecip.html>, 2020., 2021.
- 405 England, J. F., Cohn, T. A., Faber, B. A., Stedinger, J. R., Thomas, W. O. J., Veilleux, A. G., Kiang, J. E. and Mason, R. R. J.: Guidelines for Determining Flood Flow Frequency Bulletin 17C (ver 1.1, May 2019), in *U.S. Geological Survey Techniques and Methods*, book 4, 2019.
- 410 Gaál, L., Szolgay, J., Kohnová, S., Hlavčová, K., Parajka, J., Viglione, A., Merz, R. and Blöschl, G.: Dependence between flood peaks and volumes: a case study on climate and hydrological controls, *Hydrol. Sci. J.*, <https://doi.org/10.1080/02626667.2014.951361>, 2015.
- 415 Hall, J., Arheimer, B., Borga, M., Brázdil, R., Claps, P., Kiss, A., Kjeldsen, T. R., Kriaučiūnienė, J., Kundzewicz, Z. W., Lang, M., Llasat, M. C., Macdonald, N., McIntyre, N., Mediero, L., Merz, B., Merz, R., Molnar, P., Montanari, A., Neuhold, C., Parajka, J., Perdigão, R. A. P., Plavcová, L., Rogger, M., Salinas, J. L., Sauquet, E., Schär, C., Szolgay, J., Viglione, A. and Blöschl, G.: Understanding flood regime changes in Europe: A state-of-the-art assessment, *Hydrol. Earth Syst. Sci.*, <https://doi.org/10.5194/hess-18-2735-2014>, 2014.
- 420 Hamed, K. and Ramachandro Rao, A.: *Flood Frequency Analysis*, CRC Press LLC., 2000.
- Hirschboeck, K. K.: *Flood hydroclimatology*, *Flood Geomorphol.*, 1988.
- 425 Hodgkins, G. A., Dudley, R. W., Archfield, S. A. and Renard, B.: Effects of climate, regulation, and urbanization on historical flood trends in the United States, *J. Hydrol.*, <https://doi.org/10.1016/j.jhydrol.2019.03.102>, 2019.
- Hosking, J. R. M.: L-Moments: Analysis and Estimation of Distributions Using Linear Combinations of Order Statistics, *J. R. Stat. Soc. Ser. B*, <https://doi.org/10.1111/j.2517-6161.1990.tb01775.x>, 1990.
- 430 Hosking, J. R. . and Wallis, J. R.: *Regional Frequency Analysis: An Approach Based on L-moments*, Cambridge University Press, UK., 1997.
- Iacobellis, V., Claps, P. and Fiorentino, M.: Climatic control on the variability of flood distribution, *Hydrol. Earth Syst. Sci.*, <https://doi.org/10.5194/hess-6-229-2002>, 2002.
- 435 Ivancic, T. J. and Shaw, S. B.: Examining why trends in very heavy precipitation should not be mistaken for trends in very high river discharge, *Clim. Change*, <https://doi.org/10.1007/s10584-015-1476-1>, 2015.
- 440 Kidson, R. and Richards, K. S.: Flood frequency analysis: Assumptions and alternatives, *Prog. Phys. Geogr.*, <https://doi.org/10.1191/0309133305pp454ra>, 2005.

- Klemes, V.: Probability of extreme hydrometeorological events - a different approach, *Extrem. Hydrol. events. Proc. Int. symposium, Yokohama, 1993, 1993.*
- 445 Kottek, M., Grieser, J., Beck, C., Rudolf, B. and Rubel, F.: World map of the Köppen-Geiger climate classification updated, *Meteorol. Zeitschrift*, <https://doi.org/10.1127/0941-2948/2006/0130>, 2006.
- Madsen, H., Lawrence, D., Lang, M., Martinkova, M. and Kjeldsen, T. R.: Review of trend analysis and climate change projections of extreme precipitation and floods in Europe, *J. Hydrol.*, <https://doi.org/10.1016/j.jhydrol.2014.11.003>, 2014.
- 450 Mallakpour, I. and Villarini, G.: The changing nature of flooding across the central United States, *Nat. Clim. Chang.*, <https://doi.org/10.1038/nclimate2516>, 2015.
- 455 Marani, M. and Ignaccolo, M.: A metastatistical approach to rainfall extremes, *Adv. Water Resour.*, <https://doi.org/10.1016/j.advwatres.2015.03.001>, 2015.
- Merz, R. and Blöschl, G.: A process typology of regional floods, *Water Resour. Res.*, <https://doi.org/10.1029/2002WR001952>, 2003.
- 460 Merz, R. and Blöschl, G.: Flood frequency hydrology: 1. Temporal, spatial, and causal expansion of information, *Water Resour. Res.*, <https://doi.org/10.1029/2007WR006744>, 2008.
- Metzger, A., Marra, F., Smith, J. A. and Morin, E.: Flood frequency estimation and uncertainty in arid/semi-arid regions, *J. Hydrol.*, (590), 125254, <https://doi.org/https://doi.org/10.1016/j.jhydrol.2020.125254>, 2020.
- 465 Miniussi, A., Marani, M. and Villarini, G.: Metastatistical Extreme Value Distribution applied to floods across the continental United States, *Adv. Water Resour.*, <https://doi.org/10.1016/j.advwatres.2019.103498>, 2020.
- 470 Munoz, S. E., Giosan, L., Therrell, M. D., Remo, J. W. F., Shen, Z., Sullivan, R. M., Wiman, C., O'Donnell, M. and Donnelly, J. P.: Climatic control of Mississippi River flood hazard amplified by river engineering, *Nature*, <https://doi.org/10.1038/nature26145>, 2018.
- ORNLDAAC: World map of the Köppen-Geiger climate classification., 2021.
- 475 Peel, M. C., Finlayson, B. L. and McMahon, T. A.: Updated world map of the Köppen-Geiger climate classification, *Hydrol. Earth Syst. Sci.*, <https://doi.org/10.5194/hess-11-1633-2007>, 2007.
- Peel, M. C., Wang, Q. J., Vogel, R. M. and McMahon, T. A.: The utility of L-moment ratio diagrams for selecting a regional probability distribution, *Hydrol. Sci. J.*, 46(1), 147–155, <https://doi.org/10.1080/02626660109492806>, 2001.
- 480 Peterson, T. C., Heim, R. R., Hirsch, R., Kaiser, D. P., Brooks, H., Diffenbaugh, N. S., Dole, R. M., Giovannetone, J. P., Guirguis, K., Karl, T. R., Katz, R. W., Kunkel, K., Lettenmaier, D., McCabe, G. J., Paciorek, C. J., Ryberg, K. R., Schubert, S., Silva, V. B. S., Stewart, B. C., Vecchia, A. V., Villarini, G., Vose, R. S., Walsh, J., Wehner, M., Wolock, D., Wolter, K., Woodhouse, C. A. and Wuebbles, D.: Monitoring and understanding changes in heat waves, cold waves, floods, and droughts in the United States: State of knowledge, *Bull. Am. Meteorol. Soc.*, <https://doi.org/10.1175/BAMS-D-12-00066.1>, 2013.
- 485 Pitlick, J.: Relation between peak flows, precipitation, and physiography for five mountainous regions in the western USA, *J. Hydrol.*, [https://doi.org/10.1016/0022-1694\(94\)90055-8](https://doi.org/10.1016/0022-1694(94)90055-8), 1994.
- Robson, A. and Reed, D.: Flood Estimation Handbook, in *Statistical procedures for flood frequency estimation*, , 1999.
- 495 Salinas, J. L., Castellarin, A., Kohnová, S. and Kjeldsen, T. R.: Regional parent flood frequency distributions in Europe - Part 2: Climate and scale controls, *Hydrol. Earth Syst. Sci.*, <https://doi.org/10.5194/hess-18-4391-2014>, 2014a.

- 500 Salinas, J. L., Castellarin, A., Viglione, A., Kohnová, S. and Kjeldsen, T. R.: Regional parent flood frequency distributions in Europe - Part 1: Is the GEV model suitable as a pan-European parent?, *Hydrol. Earth Syst. Sci.*, <https://doi.org/10.5194/hess-18-4381-2014>, 2014b.
- Smith, J. A.: Representation of basin scale in flood peak distributions, *Water Resour. Res.*, <https://doi.org/10.1029/92WR01718>, 1992
- 505 U.S. Geological Survey (USGS): USGS Water Data for the Nation, <https://waterdata.usgs.gov/nwis/>, 2020.
- Villarini, G., Smith, J. A., Serinaldi, F., Bales, J., Bates, P. D. and Krajewski, W. F.: Flood frequency analysis for nonstationary annual peak records in an urban drainage basin, *Adv. Water Resour.*, <https://doi.org/10.1016/j.advwatres.2009.05.003>, 2009.
- 510 Vogel, R. M. and Fennessey, N. M.: L moment diagrams should replace product moment diagrams, *Water Resour. Res.*, <https://doi.org/10.1029/93WR00341>, 1993.
- 515 Vogel, R. M., Thomas, W. O. and McMahon, T. A.: Flood-Flow Frequency Model Selection in Southwestern United States, *J. Water Resour. Plan. Manag.*, [https://doi.org/10.1061/\(asce\)0733-9496\(1993\)119:3\(353\)](https://doi.org/10.1061/(asce)0733-9496(1993)119:3(353)), 1993.
- Vogel, R. M. and Wilson, I.: Probability Distribution of Annual Maximum, Mean, and Minimum Streamflows in the United States, *J. Hydrol. Eng.*, [https://doi.org/10.1061/\(asce\)1084-0699\(1996\)1:2\(69\)](https://doi.org/10.1061/(asce)1084-0699(1996)1:2(69)), 1996.
- 520 Wang, Q. J.: Unbiased estimation of probability weighted moments and partial probability weighted moments from systematic and historical flood information and their application to estimating the GEV distribution, *J. Hydrol.*, [https://doi.org/10.1016/0022-1694\(90\)90145-N](https://doi.org/10.1016/0022-1694(90)90145-N), 1990.
- 525 Zaman, M. A., Rahman, A. and Haddad, K.: Regional flood frequency analysis in arid regions: A case study for Australia, *J. Hydrol.*, <https://doi.org/10.1016/j.jhydrol.2012.08.054>, 2012.
- Zhang, W., Villarini, G., Vecchi, G. A. and Smith, J. A.: Urbanization exacerbated the rainfall and flooding caused by hurricane Harvey in Houston, *Nature*, <https://doi.org/10.1038/s41586-018-0676-z>, 2018.
- 530